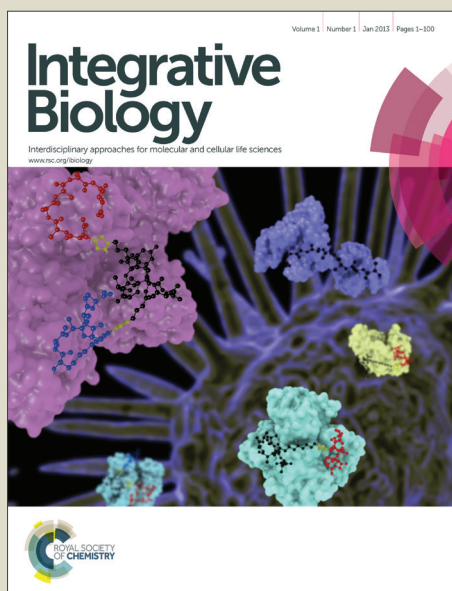


# Integrative Biology

Accepted Manuscript



This is an *Accepted Manuscript*, which has been through the Royal Society of Chemistry peer review process and has been accepted for publication.

*Accepted Manuscripts* are published online shortly after acceptance, before technical editing, formatting and proof reading. Using this free service, authors can make their results available to the community, in citable form, before we publish the edited article. We will replace this *Accepted Manuscript* with the edited and formatted *Advance Article* as soon as it is available.

You can find more information about *Accepted Manuscripts* in the [Information for Authors](#).

Please note that technical editing may introduce minor changes to the text and/or graphics, which may alter content. The journal's standard [Terms & Conditions](#) and the [Ethical guidelines](#) still apply. In no event shall the Royal Society of Chemistry be held responsible for any errors or omissions in this *Accepted Manuscript* or any consequences arising from the use of any information it contains.

## ARTICLE

## A multicellular, neuro-mimetic model to study nanoparticle uptake in cells of the central nervous system

Cite this: DOI: 10.1039/x0xx00000x

A.R. Fernandes<sup>a</sup> and D.M. Chari<sup>a</sup>Received 00th January 2012,  
Accepted 00th January 2012

DOI: 10.1039/x0xx00000x

www.rsc.org/

Evaluating the uptake and handling of biomedically relevant nanoparticles by cells of the nervous system critically underpins the effective use of nanoparticle platforms for neuro-regenerative therapies. The lack of biologically relevant and 'neuromimetic' models for nanomaterials testing (that can simulate the cellular complexity of neural tissue) currently represents a bottleneck. Further, propagation of individual cell types, in different neural cell-specific media (as commonly occurs in the nanotechnology field), can result in non-standardised corona formation around particles, confounding analyses of intercellular differences between neural cells in nanoparticle uptake. To address these challenges, we have developed a facile multicellular model that broadly simulates the ratios of neurons, astrocytes and oligodendrocytes found *in vivo*. All cell types in the model are derived from a single neural stem cell source, and propagated in the *same* medium overcoming the issue of variant corona formation. Using a fluorescent transfection-grade magnetic particle (MP), we demonstrate dramatic differences in particle uptake and resultant gene transfer between neural cell subtypes, with astrocytes being the dominant population in terms of particle uptake and transfection. We demonstrate the compatibility of the model with a high resolution scanning electron microscopy technique, allowing for membrane features of MP stimulated cells to be examined. Using this approach, astrocytes displayed high membrane activity in line with extensive particle uptake/transfection, relative to neurons and oligodendrocytes. We consider that the stem cell based model described here can provide a simple and versatile tool to evaluate interactions of neural cells with nanoparticle systems developed for neurological applications. Models of greater complexity can be evolved from this basic system, to further enhance its neuromimetic capacity.

### Introduction

Biocompatible nanoparticles are emerging as a key platform for neuro-regenerative applications, in areas such as imaging and drug/gene delivery. Testing parameters such as the uptake, stability and neurotoxicity of novel particles and obtaining functional readouts of their biomedical utility, requires access to biologically relevant and facile experimental models that simulate the cellular composition of neural tissue. The central nervous system or CNS (i.e. the brain and spinal cord) represents a special challenge in this regard- this is due to the intricate nature of CNS tissue wherein multiple cell types co-exist that possess specialised functions, morphology and biological activity. It is critical for experimental models used in nanotechnology research to take account of such biological differences, as recent studies prove these variations are reflected in dramatic differences in the uptake and handling of nanomaterials between neural cells, with major implications for neural tissue engineering.<sup>1</sup> Indeed, '*competitive uptake dynamics*' have been reported between cell sub-populations, wherein rapid/extensive nanomaterial uptake by a dominant cell type can dramatically limit uptake in other cell subtypes in the immediate neural environment.<sup>2</sup> In this context, it should be noted that current research into the uptake and handling of nanomaterials in neural cells relies overwhelmingly on the use mono-cultures, particularly those derived from cell lines. Such data is often extrapolated to the multicellular environment of the intact CNS, an approach that is

limited in its utility in light of competitive uptake dynamics that exist between neural cells.

These considerations highlight a significant current need to develop neuro-mimetic and user-friendly multicellular neural model systems for use in nanomaterials testing. Despite this need, the '*reductionist*', multicellular models described to date have several drawbacks. These largely pertain to their limited biological relevance, for example a heavy reliance on cell lines, non-uniformity of cell sources and inappropriate combinations of cells/tissue.<sup>3</sup> In this context, neural stem cells (NSCs), a multipotent population found in discrete '*germinal*' zones of the brain, could offer a novel yet simple solution for studying intercellular differences in neural cell uptake of nanoparticles. These cells have the capacity to generate the three major cell types of the central nervous system - namely the neurons, astrocytes and oligodendrocytes, *in vitro* and under defined conditions. The proportions of each cell type generated from these cells *in vitro*, viz. approximately 80-85% astrocytes, 10-15% neurons and 5% oligodendrocytes, roughly mimic intercellular ratios *in vivo* (although these can vary significantly depending on anatomical region).<sup>4-6</sup> This offers a means to analyse intercellular differences in nanoparticle handling by these cells, within a single culture system.

A major parameter to account for whilst studying intercellular differences in nanoparticle uptake is the biomolecular '*protein*

*corona* formed around particles in biological media.<sup>7</sup> The corona is a critical determinant of nanoparticle interactions with cell membrane.<sup>8</sup> Variant corona formation in different neural cell-specific media (used widely to propagate different cell types) makes it highly problematic to distinguish differences in particle uptake due to biological differences between cells, from those due to different coronas. Consequently, data obtained from isolated purified neural cell cultures propagated in distinct cell media, is of limited utility in predicting nanoparticle fate in mixed neural cell populations as exist *in vivo*. As a solution to this challenge, the daughter cells of NSCs can be maintained in the same biological medium for several days, offering a critical advantage for corona standardisation and nanomaterials testing.

Here, we demonstrate the utility of using a NSC based model, to study differences in nanoparticle uptake and gene transfer between stem cell-derived neurons, astrocytes and oligodendrocytes. To do this, we have added fluorescent, transfection-grade magnetic nanoparticles (MPs) that allow for nanoparticle uptake and gene transfer to be simultaneously visualised, to the '*mixed neural cultures*'. Our goals were to (i) conduct a head-to-head comparison of MP mediated transfection efficiencies between the three major neural subtypes; (ii) correlate nanoparticle uptake with transfection efficiency; and (iii) establish whether differences in membrane activity in different cell types correlate with nanoparticle uptake (and transfection) using a little known field emission scanning electron microscopy (FESEM)-based method.

## Materials and Methods

### Reagents / equipment

Cell culture reagents were from Life Technologies (Paisley, Scotland, UK) and Sigma (Poole, Dorset, UK). Human recombinant basic fibroblast growth factor (bFGF) was also from Sigma (Poole, Dorset, UK) and human recombinant epidermal growth factor (EGF) from R&D Systems Europe Ltd. (Abingdon, UK). Thermo Scientific Nunc culture dishes (non-treated surface) and tissue culture-grade plastics were from Fisher Scientific UK (Loughborough, UK). Fluorescent (rhodamine) NeuroMag magnetic particles were synthesized by OZ Biosciences, Marseille, France. The magnefect-nano 24-magnet array system was purchased from nanoTherics Ltd. (Stoke-on-Trent, UK) and comprises horizontal arrays of NdFeB magnets (grade N42) onto which 24-well cell culture plates can be placed. pMaxGFP plasmid (size 3.5kb; encodes green fluorescent protein [GFP]) was from Amaxa Biosciences (Cologne, Germany). Primary antibodies used were class III  $\beta$ -tubulin (Covance, Princeton, NJ), Myelin Basic Protein (Serotech, Kidlington, UK) and Glial Fibrillary Acid Protein (DakiCytomation, Ely, UK). Cy-3 and FITC conjugated secondary antibodies were from Jackson Immunoresearch Laboratories Ltd (Westgrove, PA, USA). Vectashield mounting medium with 4',6-diamidino-2-phenylindole (DAPI, nuclear marker) was from Vector Laboratories (Peterborough, UK).

The care and use of all animals used in the production of cell cultures were in accordance with the Animals Scientific Procedures Act of 1986 (UK).

### Particle characterisation

The formulation of fluorescent Neuromag particles is proprietary and patented by the company Oz Biosciences. The particle size range

reported by the company is 140-200nm, average 160nm with homogeneity in particle size, and the particles carrying a positive charge (Oz Biosciences, personal communication). To further characterise the particles, their hydrodynamic diameter and zeta potential in distilled water were determined using a Zetasizer Nano ZS (Malvern, UK). Particle size and shape were further examined by SEM. Particles were air-dried onto aluminium stubs and visualised uncoated using a Hitachi S4500 FESEM (Tokyo, Japan) operated at an accelerating voltage of 3kV.

### NSC culture

NSCs were maintained and expanded under growth factor (GF) stimulation according to the well characterised 'neurosphere' culture method. Briefly, NSCs, derived from the subventricular zone of neonatal CD1 mice were isolated and maintained in medium comprising a 3:1 mix of DMEM:F12 containing 2% B-27 supplement, 50 U/ml penicillin, 50 mg/ml streptomycin, 4 ng/ml heparin, 20 ng/ml bFGF and 20 ng/ml EGF. Cultures were fed every 2-3 days and neurospheres were passaged weekly by dissociation with a mix of accutase-DNaseI.

NSCs (passages 1-3) were dissociated and plated as 2D monolayers (MLs) on polyornithine/laminin coated coverslips, and maintained in ML medium (1:1 mix of DMEM:F12 containing 1% N2 supplement, 10 ng/ml bFGF and 10 ng/ml EGF with above antibiotic and heparin concentrations). NSC differentiation into the three daughter cells was induced the following day, by replacing ML medium with differentiation medium (neurosphere medium without growth factors and addition of 0.5% fetal bovine serum) for 4-5 days before transfection, with medium changes every 2 days.

### Multicellular Transfection

Medium was replaced with fresh differentiation medium with no antibiotics (0.225ml), 2 h prior to transfection. 250ng pMaxGFP plasmid diluted in 75 $\mu$ l DMEM:F12 base medium and added to 0.62 $\mu$ l fluorescent NeuroMag and incubated at room temperature for 20 min, to allow complexes to form. The mix was added drop-wise to the cells whilst gently swirling the plate. Controls were treated with an identical volume of base medium. Plates were returned to the incubator and placed on magnefect-Nano oscillating magnetic array system with a 24-magnet array (NdFeB, grade N42; field strength of 421 $\pm$  20mT) with an oscillating frequency at 4Hz. The rationale for using the oscillating magnetic field is that application of magnetic field in conjunction with magnetic particles (the so-called 'magnetic assistive methods' or 'magnetofection technology') can significantly improve gene transfer to neural cells.<sup>9,10</sup> Our ongoing experiments demonstrate that the 4Hz frequency yields optimal results in adherent cultures of NSCs, and was therefore used to yield the best transfection outcomes in order to facilitate observations on nanoparticle uptake and gene delivery in the current study. Field application was for 30 min, followed by 30 min in the absence of a magnetic field before replacing with differentiation medium with no antibiotics for 24 – 48 h, before performing immunocytochemistry.

### Immunocytochemistry

For all histological analyses, cells were fixed, 24-48h post-transfection, in 4% paraformaldehyde (PFA) for 15 min at RT, followed by three washes in PBS. Samples were blocked (5% normal donkey serum in PBS-0.3% Triton-X-100) for 30 min at room temperature, followed by primary antibody incubation overnight at 4°C. The following antibodies in blocking buffer were added at the indicated dilutions: Glial fibrillary protein (GFAP -

astrocytes), 1:500,  $\beta$ -Tubulin (Tuj1 - neurons), 1:1000, myelin basic protein (MBP -oligodendrocytes), 1:200. The following day, after several washes in PBS, samples were blocked as above incubated with Cy3-labelled secondary antibody (1:200) in blocking solution at room temperature for 2 h. Samples were washed several times in PBS before mounting with Vectashield mounting medium containing DAPI.

### OTOTO staining for field emission scanning electron microscopy

For SEM, cells were fixed in 2.5% (w/v) glutaraldehyde in 0.1 M sodium cacodylate / 2 mM calcium chloride buffer (pH 7.2; SCB) for 2 h at room temperature followed by several washes in SCB. Glutaraldehyde fixation of samples was followed by OTOTO conductivity staining to enhance the ultrastructural cell membrane features (OsO<sub>4</sub> / thiocarbohydrazide / OsO<sub>4</sub> / thiocarbohydrazide / OsO<sub>4</sub>). 1% OsO<sub>4</sub> in SCB (O) was applied first for 1 h followed by thorough washing in distilled water, then saturated filtered aqueous thiocarbohydrazide (T) for 20 min, and then a further O (2 h), T (20 min) and O (2 h), with washing between each step. Finally samples were dehydrated in a graded series of ethanol, critical point dried with CO<sub>2</sub> as the transitional fluid and mounted on carbon pads onto aluminium stubs. To improve electron conductivity silver conducting paint (Agar Scientific) was used to coat the sample edges.

### Microscopic analysis and imaging

An AxioScope A1 microscope equipped with an Axio Cam ICc1 digital camera and AxioVision software (release 4.7.1, Carl Zeiss MicroImaging GmbH, Goettingen, Germany) was used for fluorescence and phase contrast analyses. Cells were identified either by fluorescence microscopy using cell-specific immunological markers, or morphologically under phase contrast microscopy. The latter was necessary in situations where immunostaining protocols resulted in loss of fluorescence signal of MPs and the inability to detect internalised particles.

Culture purity and the relative proportions of each cell type in differentiated cultures were calculated by counting the numbers of DAPI positive nuclei expressing each cell marker. Percentage transfection efficiency was determined by counting the numbers of cells co-expressing GFP and cell-specific markers. The extent of MP labelling in individual cells was determined semi-quantitatively by categorizing into three groups as previously described<sup>1</sup>: no uptake, low uptake (specks of particles visible) and high uptake (large accumulations present). A minimum of 200 cells were counted for each condition.

Membrane features were examined using a Hitachi S4500 FESEM, Tokyo, Japan, (5kV accelerating voltage) after OTOTO preparation. Four membrane features were quantified (i) pits, identified as depressions of diameter ca 150-200 nm; (ii) filopodia, identified as finger like projections on the cell surface; (iii) nanopodia, identified as finger like projections from the cell, extending on the culture substrate and relatively slender compared with filopodia; and (iv) circular ruffles, identified as rounded, cup-like projections with a translucent appearance. Pits and filopodia were expressed per unit area (area of measurement = 25 $\mu$ m<sup>2</sup>) and circular ruffles per cell. Analyses were carried out on 8 cells from three replicates (n = 3).

### Statistical analyses

Data are expressed as mean  $\pm$  SEM. The number of experiments (n) refers to the number of NSC cultures, each generated from a different litter.

## Results

### Fluorescent Neuromag particle characterisation

FESEM revealed that the particle population was relatively homogenous and round in shape, with particle size approximately 200nm in diameter (Figure 1A). Other features of the particles such as charge and polydispersity index are summarised in Figure 1B.

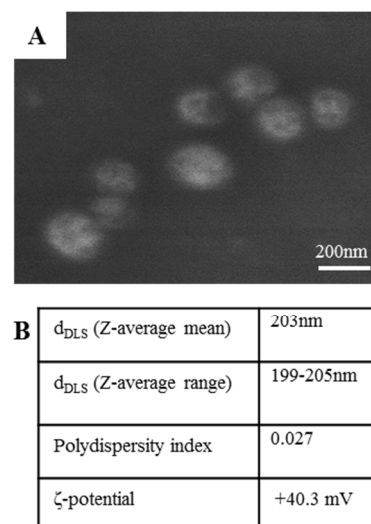


**Figure 1 Fluorescent Neuromag particle characterisation.** A) FESEM micrograph of fluorescent Neuromag particles. B) Particle size and surface charge; DLS denotes dynamic light scattering.

### MP mediated GFP transgene expression is almost exclusively restricted to astrocytes.

The parent NSC cultures from which the three neural subtypes were derived were of high purity [99.4%  $\pm$  0.036 (n=5 cultures)]. The relative ratios of differentiated astrocytes, neurons and oligodendrocytes generated in our cultures was ca 75%, 20% and 5% respectively, (n=3 cultures). Microscopic analyses revealed normal healthy cellular and nuclear morphologies for all cell types, for the duration of the experiments. The average transfection efficiency achieved overall in these cultures was 7.04%  $\pm$  1.38%. Astrocytes were found to be the predominant transfected population as most GFP<sup>+</sup> were GFAP<sup>+</sup> and either showed a flattened fibroblast-like polygonal morphology (Figure 2A) characteristic of Type 1 astrocytes or a multiple process-bearing morphology (Figure 2B) characteristic of Type 2 astrocytes. Particle associated fluorescence could be easily co-localised with GFP expression in cells (Fig 2C, arrows: Type1 astrocytes; arrowheads: Type2 astrocytes). Quantitative analyses revealed that most GFP<sup>+</sup> cells were GFAP<sup>+</sup> astrocytes (Figure 2D). Neurons were rarely transfected with only 0.4  $\pm$  0.29% GFP<sup>+</sup> cells (green) being Tuj1<sup>+</sup> (red) (Figure 2C, inset). GFP<sup>+</sup>/MBP<sup>+</sup> cells (transfected oligodendrocytes) were never observed.

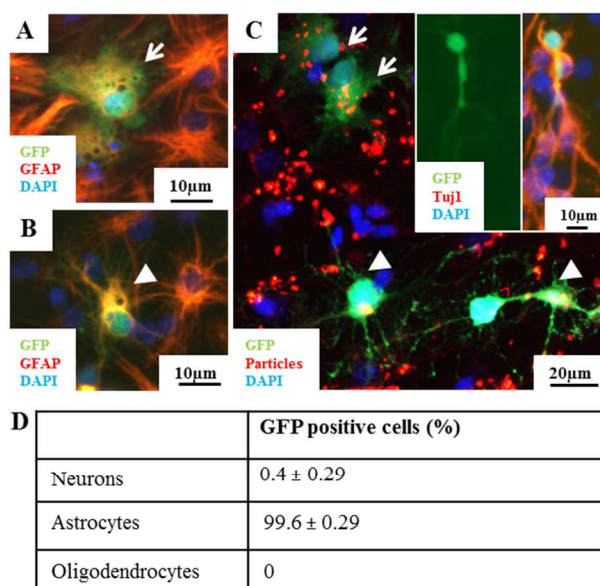


**Figure 2** Astrocytes are almost exclusively transfected in the multicellular model. Among the differentiated NSC progeny, both (A) Type I and (B) Type II astrocytes are transfected. (C) Extent of MP uptake in GFP<sup>+</sup> cells is high as observed in both astrocyte sub-types. Neurons were rarely transfected (one example shown in inset) while GFP<sup>+</sup> oligodendrocytes were never observed. (D) Table showing comparative transfection efficiencies of neurons, astrocytes and oligodendrocytes.

### Extensive magnetic particle (MP) uptake in astrocytes compared to neurons and oligodendrocytes

To correlate MP uptake with the efficiency of gene transfer, the level and extent of MP uptake between the three different cell types was assessed. Using a combination of fluorescence and phase contrast microscopy, neurons (Figure 3A) could be identified by their bipolar morphology with small nuclei (range: 40 - 55 μm<sup>2</sup>) (Figure 3B) whilst oligodendrocytes (Figure 3C) could be identified by their multiple branched and web-like processes with small (range: 50 - 65 μm<sup>2</sup>), round nuclei (Figure 3D). Astrocytes were distinguished by their comparatively large nuclei (range: 100 - 130 μm<sup>2</sup>) along with flattened or branched morphologies. Major intercellular differences were observed; particle internalisation in GFP<sup>+</sup> cells (almost exclusively possessing the morphology of astrocytes) was extensive (Figure 3E and 3F). Conversely, 93.35±2.1% cells showed extensive particle uptake and had morphologies consistent with astrocytes but were not found to express GFP despite heavy particle accumulation. No relationship could be detected between the extent of particle accumulation and transgene expression in astrocytes. In striking contrast to the pattern of particle uptake in astrocytes, both neurons (Figure 3E, arrowheads) and oligodendrocytes (Figure 3F, arrowheads) typically showed very low levels of MP accumulation, along with low or absent transfection. Semi-quantitative analysis of MP uptake in these cell types (Table in 3G) corroborated this finding.

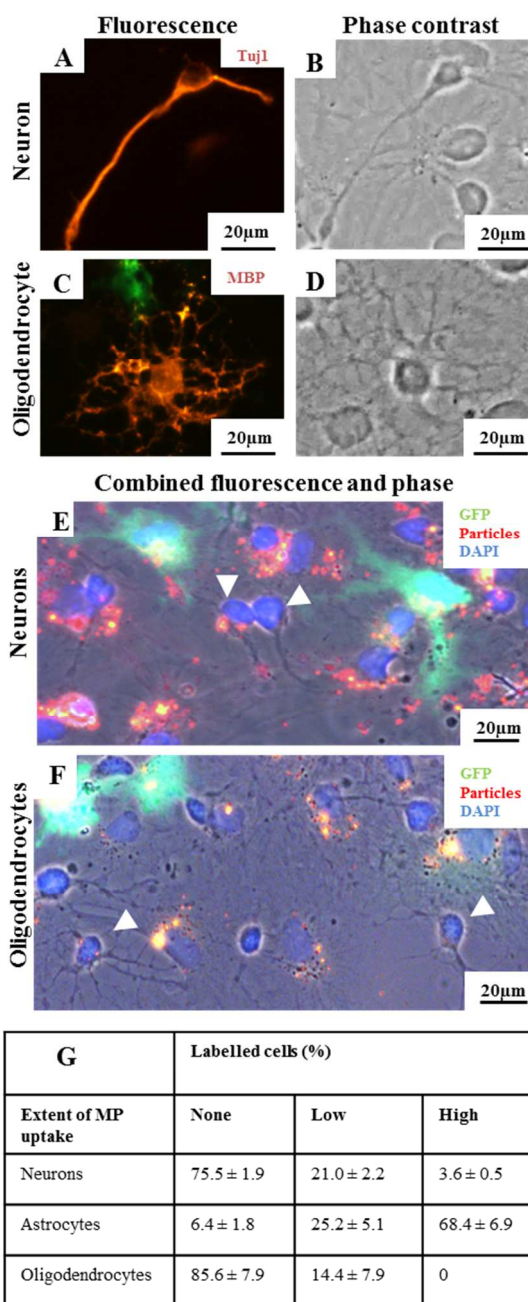


**Figure 3** Neurons and oligodendrocytes have low MP uptake compared to astrocytes. (A) Neuronal morphology revealed by TuJ1 staining and (B) phase contrast. (C) Oligodendrocyte morphology revealed by MBP staining and (D) phase contrast. (E) Neurons (arrowheads) show low particle uptake and limited transfection compared to astrocytes (surrounding cells). (F) Similar to neurons, oligodendrocytes (arrowheads) show low particle uptake and no transfection, compared with neighbouring astrocytes. (G) Comparative semi-quantitative analysis of extent of magnetic particle uptake by neurons, astrocytes and oligodendrocytes.

## Scanning electron microscopy (SEM) analysis of cell membrane activity

A comparison of the level of MP-induced membrane activity was carried out to attempt to correlate intercellular difference in transfection/particle uptake with relative cell membrane activity. Using field emission scanning electron microscopy (FESEM), all three cell types were easily distinguished by their distinctive morphologies. At low magnification, FESEM of ultrastructural topology of cell membranes revealed that astrocytes have a highly active cell membrane compared to neurons and oligodendrocytes (Figure 4A, C, E). Higher magnification revealed a higher number of pits and filopodia (Figure 4D) in astrocytes compared with neurons and oligodendrocytes (Figure 4B and F). There were no significant differences in the numbers of circular ruffles in the different cell populations. Table 4G shows a quantitative cross-cellular comparison of the cell membrane features analysed using a three-point classification system developed here.

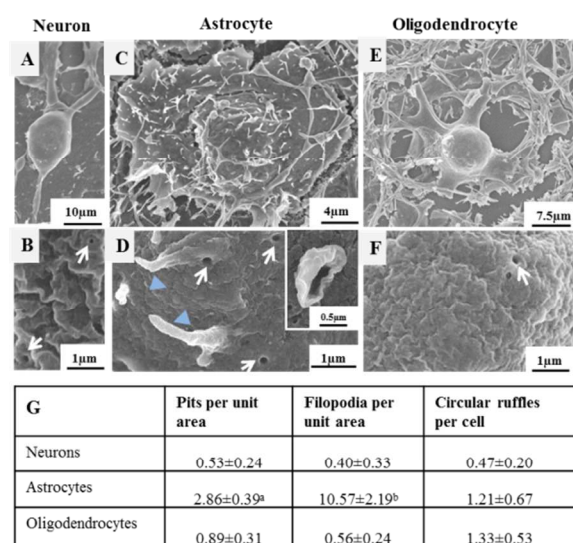


**Figure 4** A cross-cellular comparison of membrane activity in scanning electron microscopy. Low and high resolution FESEM micrographs of a neuron (A) with a relatively inactive cell membrane (B), an astrocyte (C) with a very active membrane (D) and an oligodendrocyte (E) with a comparatively inactive membrane (F). G) Quantitative analyses of membrane activity in the different cell types with astrocytes showing a higher number of pits (arrows) and filopodia (arrowheads) and circular ruffles (inset), using a 3-point classification system. <sup>a</sup>*p*<0.05; <sup>b</sup>*p*<0.001 vs neurons and oligodendrocytes (one-way ANOVA and Bonferroni's MCT). Unit area is defined as 25µm<sup>2</sup>.

## Discussion

We have successfully demonstrated the utility of a facile, NSC based model to *simultaneously* study magnetic particle uptake and gene delivery in the three major CNS cell types. This multicellular neural model offers critical advantages as a robust tool to standardise the study of particle uptake in neural cells for neurological applications (summarised in Figure 5). We further consider this model has key features that allow it to function as a useful screening tool for future nanoparticle studies to evaluate particle handling, in order to develop neurocompatible particles and to evaluate targeting strategies to direct particle uptake to specific neural cell types.

First, primary neural stem cells are isolated from a single source (subventricular zone of neonatal mice), eliminating variability in derivation of cells. Second, a standardised differentiation protocol is used to reproducibly obtain defined ratios of neurons, astrocytes and

oligodendrocytes, roughly mimicking their relative proportions *in vivo*,<sup>4-6</sup> highlighting the model's neuromimetic capacity. Third, direct intercellular comparisons of particle uptake are not feasible when individual cell types are grown in different media, due to variant corona formation. Our multicellular model has circumvented this issue by maintaining all cell types in a *single*, biologically defined medium wherein all cells encounter the same nanoparticle-corona complexes. Fourth, the model is compatible with several imaging approaches such as standard fluorescence, confocal, time lapse, scanning and transmission electron microscopy, highlighting its versatility and user-friendly nature. Finally, the model is technically simple and highly reproducible, making this an attractive option for studying nanoparticle interactions with neural cells. The model currently lacks the immune cells of the brain (the microglia). Future models will need to take account of this cell population, as our previous work has shown that rapid particle uptake by microglia (and extensive subsequent breakdown) can dramatically limit particle uptake by other neural cells,<sup>1</sup> thereby forming a major 'extracellular barrier'. Our goal in the current study is to utilise the model to reveal intercellular differences in MNP-mediated transfection between CNS cell populations (and correlate this with MNP uptake). Therefore addition of microglia would not have permitted the study objectives to be achieved. However, for specific applications, for example to use the model to evaluate particles that can evade immune components such as the widely used 'stealth coatings' for neurological applications, microglial cells can be derived from the murine CNS using simple protocols<sup>11</sup> and added to the model, highlighting the potential to further enhance its complexity and neuromimetic potential.

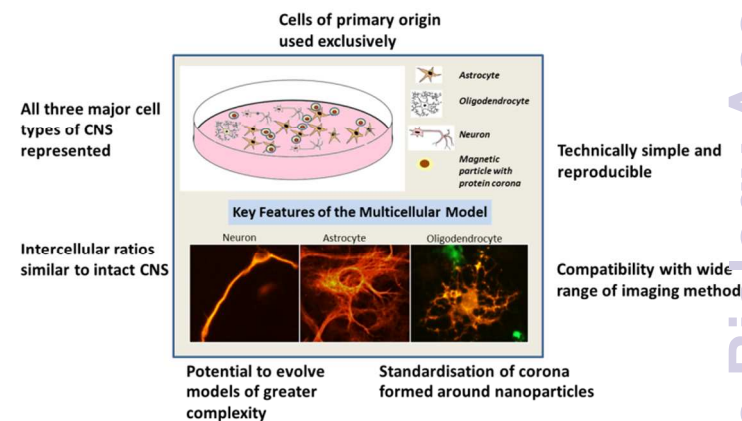


**Figure 5:** Schematic diagram of our multicellular culture model. (i) Showing its benefits for studying nanoparticle interactions with neural cells. (ii) Illustrating a multicellular model that enables accurate inter-cellular comparison of magnetic particle uptake. Particles and their associated protein corona are not drawn to scale.

Data from the model confirm the concept of '*cellular hierarchies*' in respect of nanoparticle uptake. Astrocytes (the major homeostatic cells of the CNS whose primary role is to regulate extracellular substances), overwhelmingly dominated particle uptake profiles, as would have been predicted from our earlier study using isolated cultures of astrocytes and other neural cells.<sup>1</sup> Neurons and oligodendrocytes -cells with specialist roles in neural transmission and myelin genesis respectively but with limited homeostatic functions, showed relatively little particle uptake. We consider the astrocytic dominance highlights the biological validity of our model in mimicking the distinct physiological functions of the different neural cell classes. We exploited a high resolution, OTOTO-FESEM technique to establish if intercellular differences in membrane activity could explain the observed differences in particle uptake. To the best of our knowledge, this method has never been applied to

evaluate neural cell membrane responses to nanoparticles. Using this method, the resolution of FESEM is enhanced by sequential-repeat staining of cells using osmium tetroxide (O) and a high-affinity osmium binding agent, thiocarbonylhydrazide (T).<sup>12</sup> OTOTO makes cells electron-conductive,<sup>13,14</sup> allowing for observation of finer structural detail than standard gold coating,<sup>15</sup> whilst removing the need for specialised equipment required to produce coatings like chromium/platinum.<sup>16</sup> Three categories of membrane response were easily identified in nanoparticle treated cells and quantified by OTOTO-FESEM; these responses are likely related to membrane particle trafficking. For example, membrane pits mediate MP uptake,<sup>17</sup> filopodia are cellular sensors for extracellular materials<sup>18</sup> and circular dorsal ruffles are likely related to macropinocytosis.<sup>19</sup> Our OTOTO analyses reveal the highly activated nature of astrocyte membranes, with neurons and oligodendrocytes appearing relatively quiescent - these differences can provide a reasonable explanation for cell-specific differences in particle uptake and subsequent gene transfer observed in the current study. It is of note that using the versatile OTOTO methodology, we have proven that it is possible to study the morphology and membrane features of all the cell types *simultaneously* and with high resolution, on a single cover slip, offering significant advantages of ease and high throughput.

In terms of transfection levels, the proportions of transfected astrocytes observed in the multicellular model was significantly lower than that observed in isolated cultures (7% versus 55%).<sup>20</sup> The reasons for this lowered transfection efficiency are not clear but do indicate that findings from isolated culture systems provide significant over-estimates of outcomes using nanoparticle platforms in multicellular environments, such as the intact nervous system. A further observation from this study is that the vast majority of astrocytes (ca 93%) show particle uptake without resultant transfection, even in situations where particle uptake is deemed 'high'. This suggests that the extent of particle uptake in neural cells alone is not a robust predictor of transfection outcomes. Again, it is not clear which mechanisms account for this lack of correlation. Parameters such as intracellular degradation of particle-plasmid complexes, particle sequestration into intracellular vacuoles and altered uptake dynamics and membrane properties in the presence of other cell types, cannot be ruled out at this stage.

In terms of the other cell types, previous reports suggest that MP mediated transfection efficiencies of ca 45% and 4% can be achieved in *pure* cultures of neurons<sup>21</sup> and oligodendrocytes<sup>22</sup> respectively. By contrast, low particle accumulation with negligible transfection in neurons/oligodendrocytes was observed in our multicellular model. The likely explanation for this difference is the high membrane activity and particle sequestration in astrocytes, identifying competitive intercellular uptake dynamics in *mixed neural populations* as a significant barrier to nanoparticle use in target cells such as neurons/oligodendrocytes. Strategies will need to be devised to overcome astrocyte competition, in order to achieve particle delivery to non-astrocytic neural components; future work will need to consider the use of cell targeting strategies using specific ligands, in order to overcome such competitive uptake processes, particularly in light of the fact that astrocytes are typically highly reactive in sites of neural pathology.

## Conclusions

In conclusion, we demonstrate that the stem cell based model described here can provide a simple and versatile tool to

evaluate the interactions of neural cells with a wide range of nanoparticle systems developed for neurological applications.

## Acknowledgments

This work is supported by a grant from the Biotechnology and Biomedical Sciences Research Council – BB/J017590/1.

## Notes and references

<sup>a</sup> Cellular and Neural Engineering Group, Institute for Science and Technology in Medicine, Keele University, Keele, Staffordshire, United Kingdom

1. S. I. Jenkins, M. R. Pickard, D. N. Furness, H. H. P. Yiu, and D. M. Chari, *Nanomedicine (London, England)*, 2013, **8**, 951–68.
2. J. Pinkernelle, P. Calatayud, G. F. Goya, H. Fansa, and G. Keilhoff, *BMC Neuroscience*, 2012, **13**, 32–45.
3. J. M. Breier, K. Gassmann, R. Kayser, H. Stegeman, D. De Groot, E. Fritsche, and T. J. Shafer, *Neurotoxicology and Teratology*, 2010, **32**, 4–15.
4. F. Doetsch, *Nature Neuroscience*, 2003, **6**, 1127–1134.
5. S. C. Noctor, V. Martínez-Cerdeño, and A. R. Kriegstein, *Archives of Neurology*, 2007, **64**, 639–642.
6. E. M. Ullian, S. K. Sapperstein, K. S. Christopherson, and B. A. Barres, *Science (New York, N.Y.)*, 2001, **291**, 657–661.
7. M. Xu, J. Li, H. Iwai, Q. Mei, D. Fujita, H. Su, H. Chen, and N. Hanagata, *Scientific Reports*, 2012, **2**, 406.
8. G. Maiorano, S. Sabella, B. Sorce, V. Brunetti, M. A. Malvindi, R. Cingolani, and P. P. Pompa, *ACS nano*, 2010, **4**, 7481–7491.
9. S. I. Jenkins, M. R. Pickard, N. Granger, and D. M. Chari, *ACS Nano*, 2011, **5**, 6527–38.
10. C. F. Adams, M. R. Pickard, and D. M. Chari, *Nanomedicine : Nanotechnology, Biology, and Medicine*, 2013, **9**, 737–41.
11. T. S. Bronstein R, Torres L, Nissen JC, *Journal of Visualised Experiments*, 2013, 78.
12. R. A. Vriend and H. D. Geissinger, *Journal of microscopy*, 1980, **120**, 53–64.
13. L. Keeley, *Comparative Biochemistry and Physiology*, 1973, **46**, 147–150.
14. L. E. Malick and R. B. Wilson, *Stain technology*, 1975, **50**, 265–269.
15. D. N. Furness and C. M. Hackney, *Hearing research*, 1985, **18**, 177–188.

## Journal Name

16. G. T. Belz and G. J. Auchterlonie, *Micron (Oxford, England : 1993)*, 1995, **26**, 141–144.
17. V. B. Bregar, J. Lojk, V. Suštar, P. Veranič, and M. Pavlin, *International Journal of Nanomedicine*, 2013, **8**, 919–31.
18. C. A. Heckman and H. K. Plummer, *Cellular signalling*, 2013, **25**, 2298–311.
19. J.-L. Hoon, W.-K. Wong, and C.-G. Koh, *Molecular and Cellular Biology*, 2012, **32**, 4246–4257.
20. M. R. Pickard and D. M. Chari, *Nanomedicine UK*, 2010, **5**, 217 - 232
21. C. Fallini, G. J. Bassell, and W. Rossoll, *Molecular Neurodegeneration*, 2010, **5**, 17–25.
22. S. I. Jenkins, M. R. Pickard, and D. M. Chari, *Nano LIFE*, 2013, **03**, 6527–6538.